Proposal for efficient two-dimensional atom localization using probe absorption in a microwave-driven four-level atomic system

Chunling Ding,[1,*] Jiahua Li,[1,†] Xiaoxue Yang,[1] Duo Zhang,[1,2] and Hao Xiong[1]

[1]*Wuhan National Laboratory for Optoelectronics and School of Physics, Huazhong University of Science and Technology, Wuhan 430074, People's Republic of China*

[2]*Department of Mathematics and Physics, Wuhan Polytechnic University, Wuhan 430023, People's Republic of China*

(Received 19 June 2011; published 24 October 2011)

The behavior of two-dimensional (2D) atom localization is explored by monitoring the probe absorption in a microwave-driven four-level atomic medium under the action of two orthogonal standing-wave fields. Because of the position-dependent atom-field interaction, the information about the position of the atom can be obtained via the absorption measurement of the weak probe field. It is found that the localization behavior is significantly improved due to the joint quantum interference induced by the standing-wave and microwave-driven fields. Most importantly, the atom can be localized at a particular position and the maximal probability of finding the atom in one period of the standing-wave fields reaches unity by properly adjusting the system parameters. The proposed scheme may provide a promising way to achieve high-precision and high-resolution 2D atom localization.

DOI: 10.1103/PhysRevA.84.043840 PACS number(s): 42.50.Gy

I. INTRODUCTION

The effects of atomic localization have been extensively discussed in the field of precision position measurement of an atom via different optical techniques [1–4]. Earlier schemes for the localization mainly involve one-dimensional (1D) atom localization based on the atomic coherence and quantum interference effects [5–7]. Quantum coherence and interference are so fundamental that they cover many different aspects of atomic physics and quantum optics, such as atom-field interactions [8,9], the theory of measurement [10,11], giant Kerr nonlinearities [12,13], and so on. A variety of schemes have been proposed for 1D atom localization through quantum interference. For example, Kien *et al.* [14] investigated the position localization of a polarized atom interacting with an off-resonant quantized standing-wave field. Paspalakis and Knight [15] proposed a localization scheme for an atom in a standing-wave field via quantum interference. Qamar *et al.* [16] presented a scheme of atom localization based on resonance fluorescence from a standing-wave field. Subwavelength atom localization via amplitude and phase control of the absorption spectrum has been reported in Refs. [17,18]. Also, 1D atom localization can be realized via dual measurement of the field and the atomic internal state [19], phase and amplitude control of the driving field [20,21], or interference of dark resonances [22]. In addition to these theoretical studies, the localization of an atom is already accessible experimentally with all-optical techniques [23,24]. More recently, atom localization has been demonstrated in a proof-of-principle experiment using the technique of electromagnetically induced transparency (EIT) [25]. The behavior of atom localization has attracted so much attention mainly because of its potential applications in laser cooling and trapping of neutral atoms [26,27], atom nanolithography [28,29], Bose-Einstein condensation [30,31], and measurement of the center-of-mass wave function of moving atoms [32,33].

In recent years, some schemes have been put forward for two-dimensional (2D) atom localization by applying two orthogonal standing-wave laser fields. For instance, a scheme for 2D atom localization was proposed by Ivanov and Rozhdestvensky using the measurement of the population in the upper state or in any ground state in a four-level tripod system under an influence of two orthogonal standing-wave fields [34]. Another three related 2D localization schemes have been studied by Wan and coworkers via controlled spontaneous emission from a driven tripod system [35], quantum interference in a coherently driven inverted-Y system [36], and interacting double-dark resonances in an N-type atomic system [37]. In addition, atom nanolithography based on 2D atom localization has been achieved in Ref. [38] by measuring the probe absorption. High precision and high resolution in 2D atom localization can be obtained in these schemes. However, to the best of our knowledge, so far the maximum probability of finding an atom at a particular position in a wavelength domain is 1/2. It leads us to pose the next question: can we obtain a 100% probability of finding the atom at a particular position within one period of standing-wave fields?

In order to answer the above question, here we put forward a scheme to realize 2D atom localization based on the measurement of absorption of a weak probe field in a four-level Y-type atomic system. The hyperfine transition within the excited states is resonantly coupled by means of a microwave-driven field. Of particular interest is the application of the microwave field, since the microwave source is more readily available and easier to control than an extra laser field. Moreover, one such atomic model has been used to realize the control of one- and two-photon absorption [39] and simulation of multiple spontaneously generated coherence [40]. By adjusting the system parameters, some interesting localization patterns, such as craterlike, spikelike, bicycliclike, and hill-like patterns, can be observed under the joint actions of the standing-wave and microwave-driven fields. On the one hand, when the two orthogonal standing-wave laser fields are

*clding2006@126.com

†Author to whom correspondence should be addressed: huajia_li@163.com

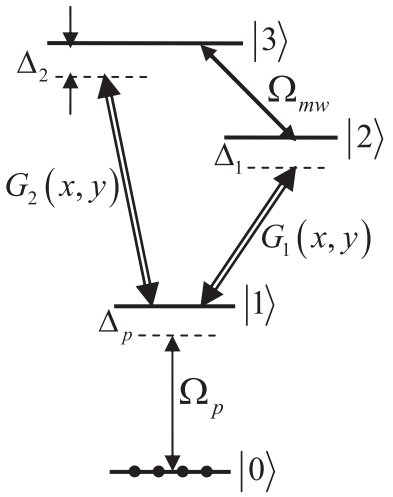

FIG. 1. Schematic diagram of a four-level Y-type atomic system, which consists of two excited levels $|2\rangle$ and $|3\rangle$, an intermediate level $|1\rangle$, and a ground level $|0\rangle$. The transitions $|1\rangle \overset{G_1(x,y)}{\longleftrightarrow} |2\rangle \overset{\Omega_{mw}}{\longleftrightarrow} |3\rangle \overset{G_2(x,y)}{\longleftrightarrow} |1\rangle$ form a cyclic configuration, in which $G_1(x,y)$ is a standing-wave field or a composition of two orthogonal standing waves, $G_2(x,y)$ is a standing-wave or a traveling-wave field, and Ω_{mw} is one-half Larmor frequency for the relevant transition. Δ_1 and Δ_2 are the frequency detunings of the corresponding standing-wave or traveling-wave fields. A weak probe laser field with Rabi frequency $2\Omega_p$ and detuning Δ_p is applied to couple the transition $|0\rangle \leftrightarrow |1\rangle$. All parameters are in units of γ.

respectively applied to couple the different atomic transitions, i.e., $G_1(x,y) = \Omega_1 \sin(k_1 x)$ and $G_2(x,y) = \Omega_2 \sin(k_2 y)$ in Fig. 1, we find that the precision and spatial resolution of the atom localization are gradually enhanced with an increase in the probe detuning under the condition that the two standing-wave fields are resonant with their respective transitions. Besides, the position of the localized atom is dependent on the phase of the microwave-driven field. On the other hand, when the two standing-wave fields are used to drive the same atomic transition, i.e., $G_1(x,y) = \Omega_1[\sin(k_1 x) + \sin(k_1 y)]$ and $G_2(x,y) = \Omega_2$, the atom can be localized at a particular position as long as the probe detuning is adjusted to an appropriate value. In this case, the probability of finding the atom in one period of the standing-wave fields is 100%; this is the main advantage in the present scheme because it doubles the probability of finding the atom at a particular position for a probe-absorption measurement compared with the previous proposed schemes [35,37]. Furthermore, our proposed scheme is based on the measurement of the probe absorption, which is much easier to realize in the practical experiment than the spontaneous-emission measurement scheme. Because spontaneous emission is a random process, the frequency of the spontaneously emitted photon is hard to control. Finally, it should be noted that these investigations may improve the localization precision and spatial resolution of the atom under certain conditions, and may provide a possibility of making the atom localized at a given position by varying the system parameters. Therefore, our scheme has more advantages than other schemes for 2D atom localization.

This paper is organized as follows. In Sec. II, we present the physical model and its theoretical description. In terms of perturbation expansion, we further derive an explicit analytical expression for the absorption of the weak probe field in the Raman-Nath approximation based on the density-matrix equations. In Sec. III, we give a detailed analysis and explanation for the behavior of 2D atom localization. Finally, we summarize our results in Sec. IV.

II. 2D ATOM LOCALIZATION SCHEME

We consider a four-level Y-type atom with two high-lying excited levels $|2\rangle$ and $|3\rangle$, one intermediate level $|1\rangle$, and a ground level $|0\rangle$, as depicted in Fig. 1. A weak probe field with a carrier frequency ω_p and a Rabi frequency $2\Omega_p$ is used to drive the transition from the intermediate level $|1\rangle$ to the ground level $|0\rangle$. An extra microwave-driven field with a Larmor frequency $2\Omega_{mw}$ is used to resonantly couple the two hyperfine levels $|2\rangle$ and $|3\rangle$ through an allowed magnetic dipole transition. The intermediate level $|1\rangle$ is simultaneously coupled to the excited levels $|2\rangle$ and $|3\rangle$ by two coherent laser fields with Rabi frequencies $G_1(x,y)$ and $G_2(x,y)$, respectively. Here, we consider two cases in which the atom interacts with the standing-wave laser fields. The first case is that $G_1(x,y)$ and $G_2(x,y)$ correspond, respectively, to the two orthogonal standing-wave fields that couple the different atomic transitions, i.e., $G_1(x,y) = \Omega_1 \sin(k_1 x)$ and $G_2(x,y) = \Omega_2 \sin(k_2 y)$, with $k_1 = \omega_1/c$ and $k_2 = \omega_2/c$ being the wave vectors of the two laser fields. The next case is that $G_1(x,y)$ corresponds to the combination of two orthogonal standing-wave fields with the same frequency that drives simultaneously the transition $|1\rangle \leftrightarrow |2\rangle$, while $G_2(x,y)$ corresponds to a traveling-wave field, that is, $G_1(x,y) = \Omega_1[\sin(k_1 x) + \sin(k_1 y)]$ and $G_2(x,y) = \Omega_2$. An atom moves in the z direction and passes through the intersectant region of the two orthogonal standing-wave fields in the x-y plane. As a result, the interaction between the atom and the standing-wave fields is spatially dependent on the x-y plane. Here we assume that the center-of-mass position of the atom along the directions of the standing-wave fields is nearly constant and we can neglect the kinetic part of the atom in the Hamiltonian by applying the Raman-Nath approximation [41]. Under these assumptions, the resulting interaction Hamiltonian, which describes the dynamics of this system in the electric dipole approximation (EDA) and the rotating-wave approximation (RWA), can be written in the form

$$\begin{aligned} H/\hbar = &-\Delta_p|1\rangle\langle 1| - (\Delta_p + \Delta_1)|2\rangle\langle 2| - (\Delta_p + \Delta_2)|3\rangle\langle 3| \\ &+[\Omega_p|0\rangle\langle 1| + G_1(x,y)|1\rangle\langle 2| + G_2(x,y)|1\rangle \\ &\times \langle 3| + \Omega_{mw}|2\rangle\langle 3| + \text{H.c.}], \end{aligned} \tag{1}$$

where the symbol H.c. represents the Hermitian conjugate. The quantities $\Delta_p = \omega_p - \omega_{10}$, $\Delta_1 = \omega_1 - \omega_{21}$, and $\Delta_2 = \omega_2 - \omega_{31}$ stand for the frequency detunings of the coherent laser fields from the corresponding atomic resonance frequencies. Here Ω_p and Ω_{mw} are one-half Rabi and Larmor frequencies for the relevant driven transitions, i.e., $\Omega_p = \mu_{10} E_p/(2\hbar)$ and $\Omega_{mw} = \mu_{32} B_{mw}/(2\hbar)$, with $\mu_{jk} = \vec{\mu}_{jk} \cdot \vec{e}_L$ ($\vec{e}_L$ is the unit polarization vector of the corresponding laser field;

$j,k = 0-3$) denoting the dipole moment for the transition $|j\rangle \leftrightarrow |k\rangle$.

In the following calculations, we set Ω_p, Ω_1, and Ω_2 as real parameters, while Ω_{mw} is set as a complex parameter, i.e., $\Omega_{mw} = |\Omega_{mw}|e^{i\varphi}$; here φ is the phase of the microwave-driven field and may also be called the relative phase. It is quite obvious from the general structure of Fig. 1 that two possible transition pathways from state $|0\rangle$ to state $|3\rangle$ exist: $|0\rangle \xrightarrow{\Omega_p} |1\rangle \xrightarrow{\Omega_2} |3\rangle$ and $|0\rangle \xrightarrow{\Omega_p} |1\rangle \xrightarrow{\Omega_1} |2\rangle \xrightarrow{\Omega_{mw}} |3\rangle$. The role of the relative phase φ on optical-absorption characteristics of the weak probe field in such a four-level Y-type atomic system with the closed-loop structure can be explained from quantum interference induced by these two excitation channels. As a consequence, the relative phase φ can be used as a control parameter to investigate the behavior of 2D atom localization, which can also be verified by Eq. (8) below.

The dynamics of this system can be described by utilizing the density-matrix approach as

$$\dot{\rho} = -\frac{i}{\hbar}[H,\rho] - \frac{1}{2}\{\Gamma,\rho\}, \tag{2}$$

where $\{\Gamma,\rho\} = \Gamma\rho + \rho\Gamma$. In general, the decay rate is combined into Eq. (2) by a relaxation matrix Γ, which can be defined by $\langle n|\Gamma|m\rangle = \gamma_n\delta_{nm}$.

By substituting the interaction Hamiltonian given by Eq. (1) into Eq. (2), the equations of motion for the density-matrix elements can be readily obtained as

$$i\dot{\rho}_{00} = i\gamma_1\rho_{11} + \Omega_p(\rho_{10} - \rho_{01}), \tag{3a}$$

$$i\dot{\rho}_{11} = -i\gamma_1\rho_{11} + i\gamma_2\rho_{22} + i\gamma_3\rho_{33} + \Omega_p(\rho_{01} - \rho_{10}) + G_1(x,y)(\rho_{21} - \rho_{12}) + G_2(x,y)(\rho_{31} - \rho_{13}), \tag{3b}$$

$$i\dot{\rho}_{22} = -i\gamma_2\rho_{22} + G_1(x,y)(\rho_{12} - \rho_{21}) + \Omega_{mw}\rho_{32} - \Omega^*_{mw}\rho_{23}, \tag{3c}$$

$$i\dot{\rho}_{33} = -i\gamma_3\rho_{33} + G_2(x,y)(\rho_{13} - \rho_{31}) + \Omega^*_{mw}\rho_{23} - \Omega_{mw}\rho_{32}, \tag{3d}$$

$$i\dot{\rho}_{10} = -\left(\Delta_p + i\frac{\gamma_1}{2}\right)\rho_{10} + \Omega_p(\rho_{00} - \rho_{11}) + G_1(x,y)\rho_{20} + G_2(x,y)\rho_{30}, \tag{3e}$$

$$i\dot{\rho}_{20} = -\left(\Delta_p + \Delta_1 + i\frac{\gamma_2}{2}\right)\rho_{20} + G_1(x,y)\rho_{10} - \Omega_p\rho_{21} + \Omega_{mw}\rho_{30}, \tag{3f}$$

$$i\dot{\rho}_{30} = -\left(\Delta_p + \Delta_2 + i\frac{\gamma_3}{2}\right)\rho_{30} + G_2(x,y)\rho_{10} - \Omega_p\rho_{31} + \Omega^*_{mw}\rho_{20}, \tag{3g}$$

$$i\dot{\rho}_{21} = -\left(\Delta_1 + i\frac{\gamma_2+\gamma_1}{2}\right)\rho_{21} + G_1(x,y)(\rho_{11} - \rho_{22}) - G_2(x,y)\rho_{23} - \Omega_p\rho_{20} + \Omega_{mw}\rho_{31}, \tag{3h}$$

$$i\dot{\rho}_{31} = -\left(\Delta_2 + i\frac{\gamma_3+\gamma_1}{2}\right)\rho_{31} + G_2(x,y)(\rho_{11} - \rho_{33}) - G_1(x,y)\rho_{32} - \Omega_p\rho_{30} + \Omega^*_{mw}\rho_{21}, \tag{3i}$$

$$i\dot{\rho}_{32} = \left(\Delta_1 - \Delta_2 - i\frac{\gamma_3+\gamma_2}{2}\right)\rho_{32} - G_1(x,y)\rho_{31} + G_2(x,y)\rho_{12} + \Omega^*_{mw}(\rho_{22} - \rho_{33}), \tag{3j}$$

where γ_1, γ_2, and γ_3 are the spontaneous decay rates from the excited state $|1\rangle$ to the ground state $|0\rangle$, from the excited state $|2\rangle$ to the excited state $|1\rangle$, and from the excited state $|3\rangle$ to the excited state $|1\rangle$, respectively. It should also be pointed out that decay rates from states $|3\rangle$ and $|2\rangle$ to state $|0\rangle$ are zero because these transitions are nondipole, which is allowed in our considered model. The relaxation rate of coherence among states $|3\rangle$ and $|2\rangle$ by collisions, etc., is negligible if we assume the cold atomic gas, and thus can be safely neglected.

Such an atomic structure can be realized in cold ^{87}Rb atoms [40,42–44] using the transitions $5S_{1/2} - 5P_{3/2} - 5D_{5/2,3/2}$. The designated states can be chosen as follows: $|0\rangle = |5S_{1/2}, F = 2\rangle$, $|1\rangle = |5P_{3/2}, F = 3\rangle$, $|2\rangle = |5D_{5/2}, F = 4\rangle$, and $|3\rangle = |5D_{3/2}, F = 3\rangle$, respectively. In this case, the decay rates of the intermediate and the excited states are $\gamma_1 = 6$ MHz and $\gamma_2 = \gamma_3 = 0.97$ MHz, respectively. In practical experiments, (i) when two standing-wave fields couple different atomic transitions, the standing-wave field $G_1(x,y)$ at a wavelength of 775.8 nm propagates in the x direction, and the standing-wave field $G_2(x,y)$ at a wavelength of 776.2 nm propagates in the y direction; and, (ii) when two standing-wave fields couple one atomic transition, $G_1(x,y)$ is the combination of two standing-wave fields with the same wavelength 775.8 nm which, respectively, propagate along the x and y directions; the traveling-wave field $G_2(x,y)$ (wavelength 776.2 nm) propagates in the x-y plane; and the weak probe field Ω_p at a wavelength of 780.2 nm propagates in the x-z plane. All of them can be obtained from the external cavity diode lasers. Here, the standing-wave field $G_1(x,y)$ interacts with the transition $|5P_{3/2}, F = 3\rangle \leftrightarrow |5D_{5/2}, F = 4\rangle$, the standing- or traveling-wave field $G_2(x,y)$ interacts with the transition $|5P_{3/2}, F = 3\rangle \leftrightarrow |5D_{3/2}, F = 3\rangle$, and the weak probe field interacts with the transition $|5S_{1/2}, F = 2\rangle \leftrightarrow |5P_{3/2}, F = 3\rangle$. The hyperfine transition $|5D_{5/2}, F = 4\rangle \leftrightarrow |5D_{3/2}, F = 3\rangle$ is coupled by a resonant microwave-driven field with frequency around 120 GHz. The value of the decay rate γ_1 in this system is 6 MHz. The magnetic dipole moment μ_{32} of the microwave-driven transition is $\frac{6+\sqrt{6}}{4}\mu_B$, with the Bohr magneton $\mu_B = 9.27 \times 10^{-24}$ J/T. For a given value of Larmor frequency, the amplitude of the microwave-driven field can be derived from the relationship $|\Omega_{mw}| = \mu_{32}B_{mw}/(2\hbar)$. Taking $|\Omega_{mw}| = 3\gamma_1$ in Fig. 4(c) as an example, the amplitude of the microwave-driven field is $B_{mw} = 2\hbar|\Omega_{mw}|/\mu_{32} = 1.92 \times 10^{-4}$ T; it is thus feasible for our proposed atomic system to be driven by the microwave field in the practical experiment. Alternatively, the probe absorption observed at appropriate frequencies is position dependent. Such position-dependent probe absorption can be reflected by a standard spectroscopic method or the heterodyne measurement of fluorescence, which may be realized via the experiment proposed in Refs. [25,45].

In the following, we will solve Eqs. (3a)–(3j) in the weak-field approximation, where the intensity of the probe field is sufficiently weak. Under the weak-field approximation, the perturbation approach can be applied to the density-matrix equations, which is introduced in terms of the perturbation expansion,

$$\rho_{jk} = \rho^{(0)}_{jk} + \lambda\rho^{(1)}_{jk} + \lambda^2\rho^{(2)}_{jk} + \cdots (j,k = 0,1,2,3), \tag{4}$$

where λ represents a continuously varying parameter ranging from zero to unity. Here $\rho_{jk}^{(0)}$ is of the zeroth order in Ω_p, $\rho_{jk}^{(1)}$ is of the first order in Ω_p, $\rho_{jk}^{(2)}$ is of the second order in Ω_p, and so on. Because our analysis is in the weak-field approximation, the atom is predominantly populated in the initial ground state $|0\rangle$. In this limit, we have $\rho_{00}^{(0)} = 1$ and others such as $\rho_{jk}^{(0)} = 0$ $(j \neq 0, k \neq 0)$ for the zeroth-order density-matrix elements. In the following calculations, we keep the terms up to the first order in the density-matrix equations. When the field is sufficiently weak, only the first-order term is important. Therefore, we only keep the first order in the probe field and keep all of the orders of the standing-wave and microwave-driven fields, which is due to the fact that these driving fields are strong fields and the probe field is very weak.

By substituting Eq. (4) into Eqs. (3a)–(3j), we can obtain the equations of motion for the first-order density-matrix element $\rho_{jk}^{(1)}$ after carrying out some algebraic calculations. Our aim in the present paper is to obtain the information about the atomic position from the susceptibility of the system at the probe frequency. Hence, in order to derive the expression of the off-diagonal density-matrix element ρ_{10}, we only need the following equations:

$$i\dot{\rho}_{10}^{(1)} = -\left(\Delta_p + i\frac{\gamma_1}{2}\right)\rho_{10}^{(1)} + G_1(x,y)\rho_{20}^{(1)} + G_2(x,y)\rho_{30}^{(1)} + \Omega_p, \tag{5a}$$

$$i\dot{\rho}_{20}^{(1)} = -\left(\Delta_p + \Delta_1 + i\frac{\gamma_2}{2}\right)\rho_{20}^{(1)} + G_1(x,y)\rho_{10}^{(1)} + \Omega_{mw}\rho_{30}^{(1)}, \tag{5b}$$

$$i\dot{\rho}_{30}^{(1)} = -\left(\Delta_p + \Delta_2 + i\frac{\gamma_3}{2}\right)\rho_{30}^{(1)} + G_2(x,y)\rho_{10}^{(1)} + \Omega_{mw}^{*}\rho_{20}^{(1)}. \tag{5c}$$

According to Eqs. (5a)–(5c), we can obtain the steady-state solutions of $\rho_{10}^{(1)}$ corresponding to the probe field. After some simple algebraic calculations, the off-diagonal density-matrix element $\rho_{10}^{(1)}$ can be given by

$$\rho_{10}^{(1)} = \frac{\Omega_p}{\Delta_p + \frac{i\gamma_1}{2} + \frac{G_1^2(x,y)(\Delta_p+\Delta_2+i\gamma_3/2)+G_2^2(x,y)(\Delta_p+\Delta_1+i\gamma_2/2)+G_1(x,y)G_2(x,y)(\Omega_{mw}+\Omega_{mw}^{*})}{|\Omega_{mw}|^2-(\Delta_p+\Delta_1+i\gamma_2/2)(\Delta_p+\Delta_2+i\gamma_3/2)}}. \tag{6}$$

The linear susceptibility of the medium for the weak probe laser field is determined by the term ρ_{10}. Consequently, the linear susceptibility can be written as [46]

$$\chi = \frac{N\mu_{01}}{\varepsilon_0 E_p}\rho_{10} = \frac{K}{\Omega_p}\rho_{10}^{(1)}, \tag{7}$$

where $K = N|\mu_{10}|^2/(2\hbar\varepsilon_0)$ with N being the atom number density in the medium and ε_0 being the permittivity in free space. Based on Eq. (7), we can straightforwardly obtain the normalized absorption for the probe field from the imaginary part of the susceptibility given as

$$\frac{\chi''(x,y;\Delta_p)}{K} = \frac{\gamma_1/2 + D/[|\Omega_{mw}|^2 - (\Delta_p+\Delta_1+i\gamma_2/2)(\Delta_p+\Delta_2+i\gamma_3/2)|^2]}{\left|\Delta_p + i\frac{\gamma_1}{2} + \frac{G_1^2(x,y)(\Delta_p+\Delta_2+i\gamma_3/2)+G_2^2(x,y)(\Delta_p+\Delta_1+i\gamma_2/2)+G_1(x,y)G_2(x,y)(\Omega_{mw}+\Omega_{mw}^{*})}{|\Omega_{mw}|^2-(\Delta_p+\Delta_1+i\gamma_2/2)(\Delta_p+\Delta_2+i\gamma_3/2)}\right|^2}, \tag{8}$$

with

$$\begin{aligned} D = {} & \tfrac{1}{2}\left[\gamma_3 G_1^2(x,y) + \gamma_2 G_2^2(x,y)\right]\left[|\Omega_{mw}|^2 - (\Delta_p+\Delta_1)(\Delta_p+\Delta_2) + \gamma_2\gamma_3/4\right] \\ & + \tfrac{1}{2}\left[\gamma_2(\Delta_p+\Delta_2) + \gamma_3(\Delta_p+\Delta_1)\right] \\ & \times \left[G_1^2(x,y)(\Delta_p+\Delta_2) + G_2^2(x,y)(\Delta_p+\Delta_1) + G_1(x,y)G_2(x,y)(\Omega_{mw}+\Omega_{mw}^{*})\right]. \end{aligned}$$

Equation (8) is the central result of the present study, which reflects the conditional position probability distribution of the atom [17,18,22,47]. It is worth noting that the analytical expression for the probe absorption is dependent on the controllable parameters of the system such as the detunings and intensities of the standing-wave driving fields, the intensity and phase of the microwave-driven field, as well as the detuning of the probe field. On the other hand, due to the fact that the normalized probe absorption depends on the position-dependent Rabi frequencies $G_1(x,y)$ and $G_2(x,y)$, it is possible to obtain the information about the position of the atom when it passes through the standing-wave fields. Moreover, the peak maxima of the probe absorption reflect the precise localization of the atom. Specifically, the peak position of the probe absorption denotes where the atom is localized, and the number of peaks in one period of the standing-wave fields means the conditional position probability. As a consequence, we can obtain the position information of the atom as it passes through the standing-wave fields by measuring the probe absorption under proper conditions.

III. RESULTS AND DISCUSSION

In this section, we discuss the conditional position probability distribution of the atom via a few numerical calculations based on the normalized probe absorption in Eq. (8), and the 2D atom localization which can be achieved by measuring the probe absorption. In the following discussion, we analyze the effect of the system parameters on the

atom localization by considering two cases. For case (i), two orthogonal standing-wave fields are, respectively, used to couple the different atomic transitions, i.e., $G_1(x,y) = \Omega_1 \sin(k_1 x)$ and $G_2(x,y) = \Omega_2 \sin(k_2 y)$; for case (ii), the two orthogonal standing-wave fields with the same frequency are applied to drive the same atomic transition, i.e., $G_1(x,y) = \Omega_1[\sin(k_1 x) + \sin(k_1 y)]$ and $G_2(x,y) = \Omega_2$. The radiative decay rate of the level $|1\rangle$ is set as $\gamma_1 = 2\gamma$. All the parameters used in this paper are in units of γ, which should be in the order of MHz for rubidium atoms.

A. Case (i): Two standing-wave fields couple different atomic transitions

First of all, we consider the case where the two orthogonal standing-wave fields couple the different atomic transitions, respectively. As can be seen from Eq. (8), it is still difficult to get the analytical solutions of the positions of the maxima of the probe absorption, even though the two standing-wave fields are both tuned to the resonant interaction with the respective atomic transitions. In Fig. 2, we give the numerical simulations and show the dependence of the normalized probe absorption versus the probe detuning Δ_p. The location of the probe-absorption peak indicates that the position of the atom is localized, while the number of peaks in one period of the standing-wave fields shows the conditional position probability. In the case of $\Delta_p = 5\gamma$, the maxima of the probe absorption are situated in the second and fourth quadrants with a latticelike pattern, as shown in Fig. 2(a). When the probe detuning is tuned to $\Delta_p = 10.3\gamma$, the localization peaks are also mainly distributed in the second and fourth quadrants of the x-y plane with little in the first and third quadrants. Moreover, the normalized probe absorption $\chi''(x,y)$ in Fig. 2(b) displays a hill-like pattern. However, when the frequency detuning of the probe field is increased to $\Delta_p = 16\gamma$, the result is completely contrary: the maxima of the absorption peaks are all located in the first and third quadrants with a

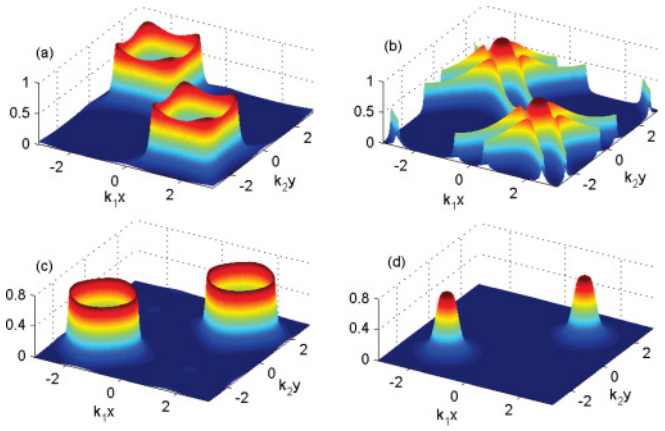

FIG. 2. (Color online) The normalized probe absorption $\chi''(x,y)$, which directly reflects the conditional position probability distribution, as a function of $(k_1 x, k_2 y)$ in dependence on the detuning Δ_p of the probe field. $\Delta_p =$ (a) 5γ, (b) 10.3γ, (c) 16γ, (d) 19.3γ. The other parameters used are $\Omega_1 = \Omega_2 = 10\gamma$, $|\Omega_{mw}| = 9\gamma$, $\Delta_1 = \Delta_2 = 0$, $\gamma_1 = 2\gamma$, $\gamma_2 = \gamma_3 = 0.32\gamma$, and $\varphi = 0$. All parameters are in units of γ.

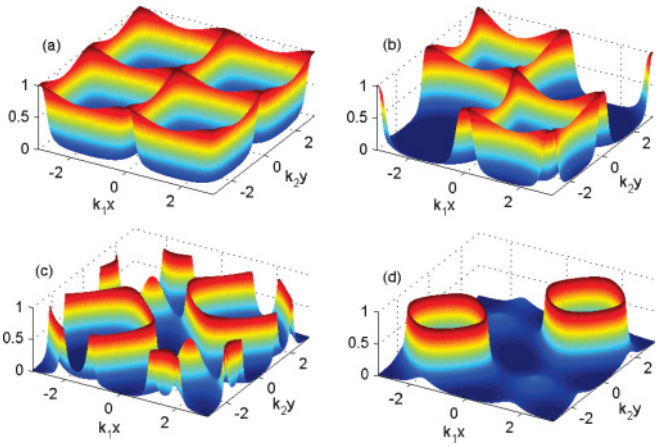

FIG. 3. (Color online) The normalized probe absorption $\chi''(x,y)$ as a function of $(k_1 x, k_2 y)$ for different combinations of the three detunings. $(\Delta_1, \Delta_2, \Delta_p) =$ (a) $(0,0,0)$, (b) $(5\gamma, 5\gamma, 0)$, (c) $(5\gamma, 5\gamma, 9.2\gamma)$, (d) $(9.8\gamma, 9.8\gamma, 9.2\gamma)$. The system parameters used are the same as Fig. 2. All parameters are in units of γ.

craterlike pattern, and the atom is localized at the circular edges of the two craters [see Fig. 2(c)]. Furthermore, when the probe detuning is detected at an appropriate value [i.e., $\Delta_p = 19.3\gamma$ in Fig. 2(d)], the resulting absorption spectrum exhibits a spikelike pattern in the first and third quadrants. In such a case, we can achieve much better spatial resolution in the conditional position probability distribution of the atom. Therefore, we can always obtain a higher probability to find the atom in two of the four quadrants by measuring the probe absorption under two-photon resonance conditions.

In Fig. 3, we plot the normalized probe-absorption spectrum $\chi''(x,y)$ versus the normalized positions $(k_1 x, k_2 y)$ by modulating the three controllable detuning parameters simultaneously. When the three laser fields are tuned resonant with the corresponding atomic transitions, i.e., $(\Delta_1, \Delta_2, \Delta_p) = (0,0,0)$, the probe absorption displays a latticelike pattern and the atom is localized around the nodes of two orthogonal standing-wave fields, as shown in Fig. 3(a). For the case that $(\Delta_1, \Delta_2, \Delta_p) = (5\gamma, 5\gamma, 0)$, the maxima of the probe absorption are mostly distributed in the second and fourth quadrants of the x-y plane, with little in the first and third quadrants [see Fig. 3(b)]. When the probe field is far detuned from the atomic transition and the values of the other two detunings are kept the same as those in Fig. 3(b) [i.e., $(\Delta_1, \Delta_2, \Delta_p) = (5\gamma, 5\gamma, 9.2\gamma)$ in Fig. 3(c)], the absorption peaks are situated in the four quadrants but with different patterns. In such a condition, the probe-absorption maxima in the first and third quadrants show a latticelike pattern, and the absorption peaks in the second and fourth quadrants display a spikelike pattern. Interestingly, when all three laser fields are far off resonance, that is, $(\Delta_1, \Delta_2, \Delta_p) = (9.8\gamma, 9.8\gamma, 9.2\gamma)$, the maxima of the probe absorption are mainly distributed in the first and third quadrants of the x-y plane with a craterlike pattern, with little in the second and fourth quadrants, as can be seen from Fig. 3(d). In this case, we can obtain a higher probability to find the atom in the standing-wave fields compared to Figs. 3(a)–3(c).

Now, let us investigate the influence of the intensity and phase of the microwave field on the behavior of 2D

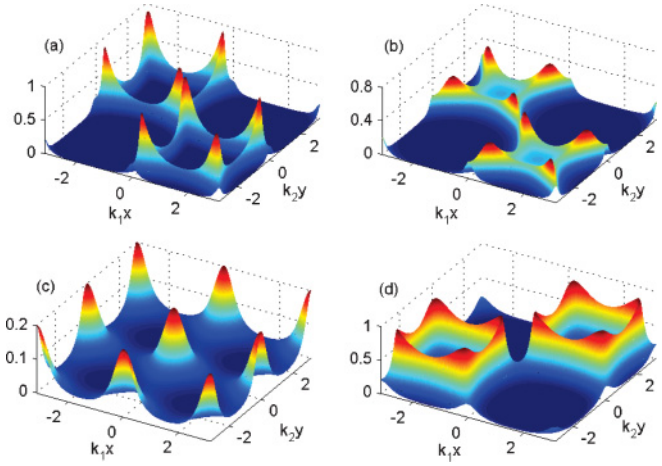

FIG. 4. (Color online) The normalized probe absorption $\chi''(x,y)$ as a function of (k_1x,k_2y) in dependence on the microwave-driven field. (a) $|\Omega_{mw}| = 3\gamma, \varphi = 0$; (b) $|\Omega_{mw}| = 3\gamma, \varphi = \pi/4$; (c) $|\Omega_{mw}| = 6\gamma, \varphi = \pi/2$; (d) $|\Omega_{mw}| = 6\gamma, \varphi = 3\pi/4$. The system parameters used are the same as Fig. 2, except that $\Delta_p = 2\gamma$. All parameters are in units of γ.

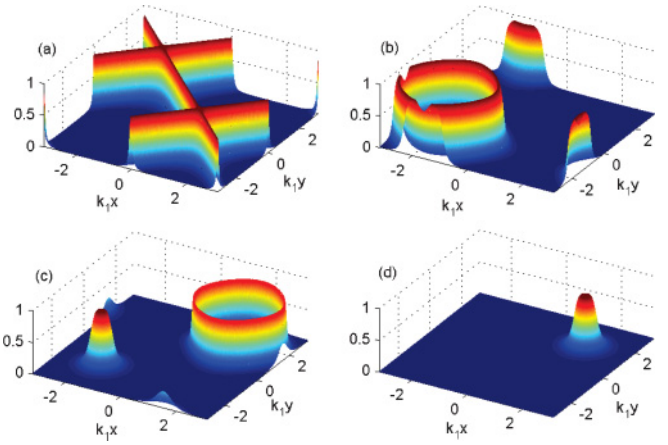

FIG. 5. (Color online) The normalized probe absorption $\chi''(x,y)$ as a function of (k_1x,k_1y) in dependence on the probe detuning Δ_p. Δ_p = (a) 0, (b) 10γ, (c) 20γ, (d) 26.7γ. The system parameters used are the same as Fig. 2. All parameters are in units of γ.

atom localization. The normalized probe-absorption spectrum $\chi''(x,y)$ is plotted in Fig. 4 as a function of the normalized positions (k_1x, k_2y) with four different sets of parameter values of the microwave field. In the case of $|\Omega_{mw}| = 3\gamma$ and $\varphi = 0$, the peak maxima of the probe absorption lie around the intersections of the nodes of the two standing-wave fields in the second and fourth quadrants of the x-y plane, as shown in Fig. 4(a). It can be seen from Fig. 4(a) that these localization peaks are very sharp, which means that one can achieve much better spatial resolution at these positions compared with Fig. 3(b). For a given intensity of the microwave field, when the phase φ is varied from 0 to $\pi/4$, the positions of the maxima of the absorption peaks remain almost unchanged, but the localization precision of the atom is decreased [see Fig. 4(b)]. However, for the case that $|\Omega_{mw}| = 6\gamma$ and $\varphi = \pi/2$, the peak maxima of the absorption spectrum are located at the intersections of the nodes of the two standing-wave fields with a spikelike pattern, as illustrated in Fig. 4(c), which is similar to Fig. 4(a) in Ref. [35] and Fig. 3(d) in Ref. [36]. When the phase φ is further varied from $\pi/2$ to $3\pi/4$, the probe-absorption maxima with latticelike patterns are distributed on the nodes of two standing-wave fields in the first and third quadrants of the x-y plane, as can be seen from Fig. 4(d), and the atom is localized at the edges of the two lattices. The conditional position probability distribution of the atom is contrary to that shown in Figs. 4(a) and 4(b) when the phase is increased by a factor of $\pi/2$.

B. Case (ii): Two standing-wave fields couple one atomic transition

In the following, we investigate the case where the two standing-wave fields drive simultaneously the same atomic transition, and the other atomic transition is coupled by a traveling-wave field, i.e., $G_1(x,y) = \Omega_1[\sin(k_1x) + \sin(k_1y)]$ and $G_2(x,y) = \Omega_2$. Figure 5 shows the effects of the probe detuning on the atom localization behavior in such a case. Since the driving and probe fields are resonant with the corresponding atomic transitions, i.e., $\Delta_1 = \Delta_2 = \Delta_p = 0$, it can be seen from Fig. 5(a) that the probe-absorption maxima are distributed on the diagonal in the second and fourth quadrants; this indicates that the atom localization peaks are determined by $k_1x + k_1y = 2m\pi$ or $k_1x - k_1y = (2n+1)\pi$ (m,n are integers). When the probe detuning is adjusted to $\Delta_p = 10\gamma$, the peak maxima of the probe absorption are situated in the second, third, and fourth quadrants, and are mainly localized in the third quadrant with a craterlike pattern [see Fig. 5(b)]. When the detuning of the probe field is tuned to an appropriate value, i.e., $\Delta_p = 20\gamma$ in Fig. 5(c), the probe-absorption maxima are distributed in the first and third quadrants with different patterns, in which the localization peaks in the first quadrant display a craterlike pattern and the localization peaks in the third quadrant exhibit a spikelike pattern with a high precision. Most interestingly, when the probe detuning is increased to $\Delta_p = 26.7\gamma$, the probe-absorption maxima are only situated in the first quadrant with a spikelike pattern and thus the atom is localized at position $(k_1x,k_1y) = (\pi/2,\pi/2)$, as shown in Fig. 5(d), and the localization peak with a spikelike pattern in the third quadrant [see Fig. 5(c)] has completely disappeared. As a matter of fact, when the probe detuning Δ_p is varied within the interval $[22\gamma,26.5\gamma]$, the localization peak with a craterlike pattern lies completely in the first quadrant. Furthermore, the localization precision is improved with an increase in the probe detuning. However, when $\Delta_p \in [26.6\gamma,29.6\gamma]$, the localization peak becomes a spikelike pattern and is still located in the first quadrant. In such a condition, the probability of finding the atom in one period of the standing-wave fields is increased from 1/2 [see Fig. 2(d)] to 1; that is to say, the atom can be localized at a particular position and the 2D atom localization is, indeed, achieved. Therefore, the probability of finding the atom at a particular position is increased by a factor of 2 or 4 compared to the previous proposed schemes [35–38]. Moreover, the localization of an atom in one specific quadrant is almost unchanged when the detuning is varied in the two intervals, $[22\gamma,26.5\gamma]$ and $[26.6\gamma,29.6\gamma]$. It can be readily verified that the change of the probe detuning within a certain

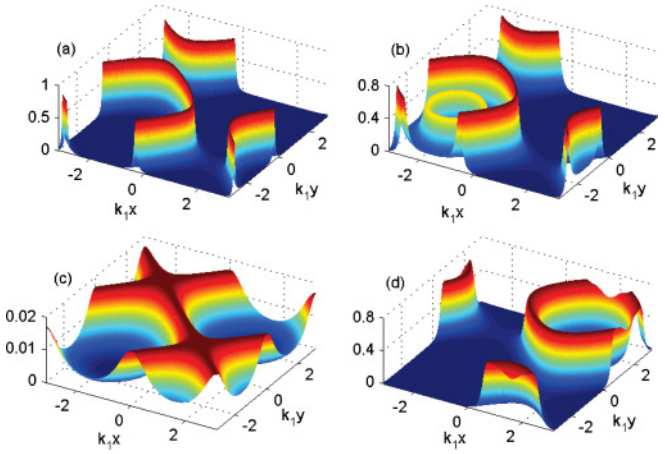

FIG. 6. (Color online) The normalized probe absorption $\chi''(x,y)$ as a function of (k_1x,k_1y) for different values of the detuning Δ_2 and the phase φ. (a) $\Delta_2 = 3\gamma$, $\varphi = 0$; (b) $\Delta_2 = 6\gamma$, $\varphi = \pi/4$; (c) $\Delta_2 = 6\gamma$, $\varphi = \pi/2$; (d) $\Delta_2 = 8\gamma$, $\varphi = 3\pi/4$. The system parameters used are the same as Fig. 2, except that $\Delta_1 = 5\gamma$ and $\Delta_p = 0$. All parameters are in units of γ.

range of parameters does not affect the result concerning the high precision and high resolution of the atom localization. This is a significant advantage of our proposed scheme.

In Fig. 6, we present the different patterns of the normalized probe absorption by varying the driving field detuning Δ_2 and the phase φ of the microwave-driven field when the probe field is tuned to the resonant interaction with the corresponding atomic transition. For the case that $\Delta_2 = 3\gamma$ and $\varphi = 0$, the probe-absorption maxima are mostly distributed in the third quadrant, with little in the second and fourth quadrants, as shown in Fig. 6(a). Furthermore, owing to the destructive quantum interference caused by the microwave-driven field, the probability of finding an atom in the standing-wave fields is improved by a factor of 2, compared with Figs. 5(a) and 5(b) in Ref. [37]. However, when $\Delta_2 = 6\gamma$ and $\varphi = \pi/4$, the localization peaks in the third quadrant exhibit a bicycliclike pattern, and the localization peaks in the second and fourth quadrants remain almost unchanged [see Fig. 6(b)]. The maxima of the probe absorption are mainly distributed on the diagonal in the second and fourth quadrants when the phase is changed from $\varphi = \pi/4$ to $\varphi = \pi/2$ [see Fig. 6(c)], which is similar to that shown in Fig. 5(a); the difference is that the degree of atom localization is decreased. Under the condition of $\Delta_2 = 8\gamma$ and $\varphi = 3\pi/4$, the probe-absorption maxima are mainly situated in the first quadrant, with little in the second and fourth quadrants, of the x-y plane, as shown in Fig. 6(d), which is the mirror reflection of the localization patterns observed in Fig. 5(b).

The aim now is to properly discuss the momentum distribution behaviors of the 2D atom localization. Under certain conditions, it is shown that a sharp single localization peak can be obtained in a subwavelength region [see, for example, Fig. 5(d)]. However, when this happens, how is the momentum distribution of the sharp single localization peak? Is such a sharp localization accompanied by a very wide momentum spread? In order to address this problem, we first carry out the Fourier transform of the normalized susceptibility given in Eq. (8), and thus we can obtain

$$F(p_x,p_y) = \int_{-\infty}^{\infty}\int_{-\infty}^{\infty} f(x,y)e^{-\frac{i}{\hbar}p_x x}e^{-\frac{i}{\hbar}p_y y}dxdy, \qquad (9)$$

where $f(x,y) = \frac{\chi''(x,y;\Delta_p)}{K}$. Based on Eq. (9), we present in Fig. 7 the corresponding momentum distribution in conjunction with the spatial distribution for the case shown in Fig. 5(d) by numerical simulations. We find that the atom can still be localized at a particular position in the momentum space. The difference between the momentum space and the position space is that the momentum spread is wider and the localization peak is not sharper than that shown in Fig. 5(d), which is originated from the uncertainty relations of position and momentum. Consider that the position and momentum are two Hermitian operators, which satisfy the commutation relation $[x,p_x] = i\hbar$. According to the Heisenberg uncertainty relation, the product of the uncertainties in determining the expectation values of position and momentum is given by [46]

$$(\Delta x)(\Delta p_x) \geqslant \frac{\hbar}{2}, \qquad (10)$$

where Δx is the root-mean-square deviation of the coordinate x, and Δp_x is the root-mean-square deviation of the momentum p_x. Similarly, we can get $(\Delta y)(\Delta p_y) \geqslant \frac{\hbar}{2}$. According to the relation between momentum and wave vector $\vec{p} = \hbar\vec{k}$, we have

$$(k_1\Delta x)(\Delta p_x) \geqslant \frac{\hbar k_1}{2}, \quad (k_1\Delta y)(\Delta p_y) \geqslant \frac{\hbar k_1}{2}. \qquad (11)$$

As a result, the uncertainty range of momentum can be represented as

$$\frac{\Delta p_x}{p_x} \geqslant \frac{1}{2k_1\Delta x}, \quad \frac{\Delta p_y}{p_x} \geqslant \frac{1}{2k_1\Delta y}. \qquad (12)$$

From Fig. 5(d) and Fig. 7, we can estimate that $\frac{\Delta p_x}{p_x} \approx \frac{1}{1.7}$, $\frac{\Delta p_y}{p_x} \approx \frac{1}{1.7}$, $\frac{1}{2k_1\Delta x} \approx \frac{1}{2}$, and $\frac{1}{2k_1\Delta y} \approx \frac{1}{2}$. As can be seen, these numerical simulation results are in complete agreement with theoretical calculations. This means that the result in Fig. 7 is reasonable within the uncertainty relations and practical

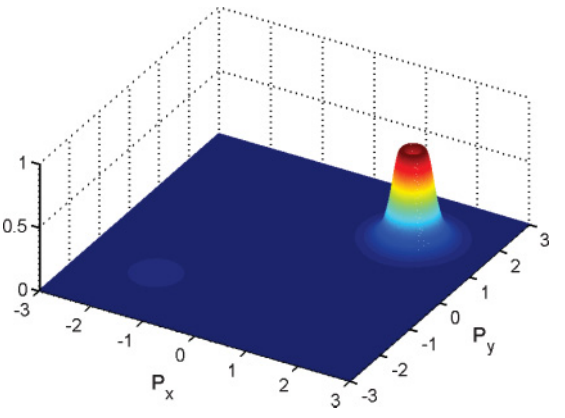

FIG. 7. (Color online) Momentum distribution of the normalized probe absorption $\chi''(x,y)$ for the case shown in Fig. 5(d). Note that P_x and P_y in the horizontal axis are in units of $\hbar k_1$. Other parameters are in units of γ.

applications. Accordingly, under certain conditions, we can obtain a sharp localization peak in the position space, while the localization peak becomes wider in the momentum space. These investigations are consistent with the basic principle of quantum mechanics. Therefore, these localization peaks can also be observed in momentum space but they are accompanied with a wide momentum spread due to the influence of the uncertainty principle. Also, it can be seen from the position-momentum uncertainty relations that the mean-square deviation of the position gets smaller and the mean-square deviation of the momentum gets larger, which means that the more precise the position distribution of an atom is, the less precise is its momentum distribution.

Before ending this section, we will give some physical explanations of the above results. On the one hand, it is clear from the above discussion that our scheme of applying a microwave field associated with two orthogonal standing-wave fields can greatly increase the detecting probability and improve the localization precision, as well as, indeed, realize the 2D atom localization in the x-y plane. It is obvious that the maxima of the probe absorption directly reflects the position probability distribution of the atom, and the standing-wave fields are dependent on the spatial position, and thus high-precision and high-resolution atom localization can be obtained by measuring the probe absorption at a particular frequency. When the phase of the microwave-driven field is equal to $(2n+1)\pi/2$ (n is an integer), it can be seen from Eq. (8) that the interference term $G_1(x,y)G_2(x,y)(\Omega_{rf}+\Omega_{rf}^*)=0$, which means that there is no quantum interference between the atomic transitions. Therefore, in this case, the atom localization behavior is similar to that shown in Refs. [35,36]. On the other hand, when the phase $\varphi=n\pi$, the interference term in Eq. (8) is $G_1(x,y)G_2(x,y)(\Omega_{rf}+\Omega_{rf}^*)=\pm 2G_1(x,y)G_2(x,y)|\Omega_{rf}|$; this means that there exists maximal quantum interference between the relevant atomic transitions. Under two-photon resonance conditions, the localization peaks are confined to two of the four quadrants as a result of the joint quantum interference effects. Especially for a large probe detuning, the atom can be localized at a given position when the two standing-wave fields drive the same atomic transition. Due to the destructive quantum interference induced by the microwave-driven field, the probability of finding the atom in one period of the standing-wave fields is doubled compared to that shown in Ref. [37] under certain conditions.

On the other hand, by using the dressed-state picture, the bare-state levels $|1\rangle$, $|2\rangle$, and $|3\rangle$ can be replaced by three dressed states, $|a\rangle$, $|b\rangle$, and $|c\rangle$ (not shown here), under the action of three driving laser fields. After some mathematical calculations, the energy eigenvalues of the three dressed states for the two-photon resonant case that $\Delta_1=\Delta_2=0$ can be obtained as

$$E_b(x,y)=\frac{1}{6}M(x,y)+\frac{2A(x,y)}{M(x,y)}, \tag{13a}$$

$$E_{a,c}(x,y)=-\left[\frac{M(x,y)}{12}+\frac{A(x,y)}{M(x,y)}\right] \pm i\frac{\sqrt{3}}{2}\left[\frac{M(x,y)}{6}-\frac{2A(x,y)}{M(x,y)}\right], \tag{13b}$$

with

$$M(x,y)=\sqrt[3]{-108B(x,y)+12\sqrt{-12A^3(x,y)+81B^2(x,y)}},$$
$$A(x,y)=G_1^2(x,y)+G_2^2(x,y)+|\Omega_{mw}|^2,$$
$$B(x,y)=G_1(x,y)G_2(x,y)(\Omega_{mw}+\Omega_{mw}^*).$$

The corresponding energy eigenstates can be written as

$$\begin{aligned}|j\rangle=&[G_1(x,y)\Omega_{mw}-G_2(x,y)E_j(x,y)]|3\rangle\\&+[G_2(x,y)\Omega_{mw}^*-G_1(x,y)E_j(x,y)]|2\rangle\\&+\left[E_j^2(x,y)-|\Omega_{mw}|^2\right]|1\rangle,\end{aligned} \tag{14}$$

where $j=a,b,c$. The origin of the localization peaks can be explained in the dressed-state representation of the standing-wave and microwave-driven fields. It can be seen from the above Eqs. (13) and (14) that the contribution of three bare-state levels to the dressed states is different; in addition, the quantum interference effects between three transition channels (from the ground level to the dressed levels) are also different from each other, and thus lead to different localization patterns and precision of an atom. When the two standing-wave fields are, respectively, applied to couple the different atomic transitions, the contribution of the bare-state levels to the dressed state $|a\rangle$ is identical to that of $|c\rangle$, and the quantum interference between $|i\rangle\leftrightarrow|0\rangle$ ($i=a,c$) and $|b\rangle\leftrightarrow|0\rangle$ leads to the probe-absorption maxima distributing equally in two of the four quadrants. However, when the probe field is tuned to the resonance with the corresponding atomic transition, the probe field is always absorbed by the atom at the position $k_1x=m\pi$ or $k_2y=n\pi$ (m,n are integers) of the x-y plane; as a result, the atom is localized around the nodes of two standing-wave fields. When the phase is equal to $\pi/2$, we have $E_b(x,y)=0$ and $E_{a,c}(x,y)=\mp\sqrt{A(x,y)}=E_{a,c}(-x,-y)$, and therefore the localization peaks distribute equally in the four quadrants. On the other hand, when the two standing-wave fields are used to drive the same atomic transition, the energy eigenvalues of the three dressed states are varied with the coordinate positions, and the probability distribution of the absorption peaks is unequal in the four quadrants. In particular, for a larger detuning of the probe field, we can find the atom at a particular position due to the combined effects of the quantum interference.

IV. CONCLUSIONS

In conclusion, we have proposed and analyzed a scheme for 2D atom localization via probe absorption in a four-level Y-type atomic system, in which the hyperfine transition between two high-lying excited levels is coupled by a resonant microwave-driven field. We have shown that the behavior of atom localization depends upon these controllable detunings of probe and standing-wave fields, as well as the parameter values of the microwave field. Some interesting localization patterns, such as craterlike, spikelike, bicyclicklike, and hill-like patterns, can be obtained by adjusting these system parameters. When two standing-wave fields are, respectively, coupled to different atomic transitions, the localization precision and spatial resolution of the atom are improved with the increase of probe detuning under two-photon resonance conditions. Moreover, we can obtain a higher probability to find the

atom in two of the four quadrants. In the case that the two standing-wave fields drive the same transition, we can make an atom localized at a particular position with high precision and high resolution when the probe detuning is tuned to an appropriate value. The main advantage of our proposed scheme is that the probability of finding the atom in one period of the standing-wave fields is 100%, which is originated from the joint quantum interference induced by the two orthogonal standing-wave fields, the traveling-wave field, and the microwave-driven field.

Finally, it should be pointed out that our scheme is based on the probe-absorption measurement, and the absorption measurement is much easier to carry out in a laboratory compared to the measurement of spontaneous emission. In our absorption-measurement scheme, the atom is prepared in the ground state, which is very easy to implement in atomic physics experiments. These advantages provide a possibility to observe 2D atom localization in the experiment.

ACKNOWLEDGMENTS

We would like to thank Professor Ying Wu for helpful discussion and encouragement. The research is in part supported by the National Natural Science Foundation of China (Grants No. 10975054, No. 91021011, and No. 11004069), the Doctoral Foundation of the Ministry of Education of China under Grant Nos. 20100142120081 and 200804870051, the Innovation Foundation from Huazhong University of Science and Technology under Grant No. 2010MS074, and the National Basic Research Program of China under Contract No. 2012CB922103.

[1] K. D. Stokes, C. Schnurr, J. R. Gardner, M. Marable, G. R. Welch, and J. E. Thomas, Phys. Rev. Lett. **67**, 1997 (1991).
[2] P. Storey, M. Collett, and D. Walls, Phys. Rev. A **47**, 405 (1993).
[3] R. Quadt, M. Collett, and D. F. Walls, Phys. Rev. Lett. **74**, 351 (1995).
[4] M. Holland, S. Marksteiner, P. Marte, and P. Zoller, Phys. Rev. Lett. **76**, 3683 (1996).
[5] H. B. Li, V. A. Sautenkov, M. M. Kash, A. V. Sokolov, G. R. Welch, Y. V. Rostovtsev, M. S. Zubairy, and M. O. Scully, Phys. Rev. A **78**, 013803 (2008).
[6] G. S. Agarwal and K. T. Kapale, J. Phys. B **39**, 3437 (2006).
[7] S. Qamar, A. Mehmood, and S. Qamar, Phys. Rev. A **79**, 033848 (2009).
[8] Y. Wu, L. L. Wen, and Y. F. Zhu, Opt. Lett. **28**, 631 (2003).
[9] J. Y. Gao, C. Guo, X. Z. Guo, G. X. Jin, Q. W. Wang, J. Zhao, H. Z. Zhang, Y. Jiang, D. Z. Wang, and D. M. Jiang, Opt. Commun. **93**, 323 (1992).
[10] H. Müller, A. Peters, and S. Chu, Nature (London) **463**, 926 (2010).
[11] Y. Wu and X. X. Yang, Phys. Rev. A **76**, 013832 (2007).
[12] H. Wang, D. Goorskey, and M. Xiao, Phys. Rev. Lett. **87**, 073601 (2001).
[13] Y. Wu and X. X. Yang, Appl. Phys. Lett. **91**, 094104 (2007).
[14] F. LeKien, G. Rempe, W. P. Schleich, and M. S. Zubairy, Phys. Rev. A **56**, 2972 (1997).
[15] E. Paspalakis and P. L. Knight, Phys. Rev. A **63**, 065802 (2001).
[16] S. Qamar, S. Y. Zhu, and M. S. Zubairy, Phys. Rev. A **61**, 063806 (2000).
[17] M. Sahrai, H. Tajalli, K. T. Kapale, and M. S. Zubairy, Phys. Rev. A **72**, 013820 (2005).
[18] K. T. Kapale and M. S. Zubairy, Phys. Rev. A **73**, 023813 (2006).
[19] H. Nha, J. H. Lee, J. S. Chang, and K. An, Phys. Rev. A **65**, 033827 (2002).
[20] F. Ghafoor, S. Qamar, and M. S. Zubairy, Phys. Rev. A **65**, 043819 (2002).
[21] J. Xu and X. M. Hu, Phys. Rev. A **76**, 013830 (2007).
[22] C. P. Liu, S. Q. Gong, D. C. Cheng, X. J. Fan, and Z. Z. Xu, Phys. Rev. A **73**, 025801 (2006).
[23] J. R. Gardner, M. L. Marable, G. R. Welch, and J. E. Thomas, Phys. Rev. Lett. **70**, 3404 (1993).
[24] L. Guidoni and P. Verkerk, Phys. Rev. A **57**, R1501 (1998).
[25] N. A. Proite, Z. J. Simmons, and D. D. Yavuz, Phys. Rev. A **83**, 041803(R) (2011).
[26] H. Metcalf and P. Van der Straten, Phys. Rep. **244**, 203 (1994).
[27] W. D. Phillips, Rev. Mod. Phys. **70**, 721 (1998).
[28] K. S. Johnson, J. H. Thywissen, W. H. Dekker, K. K. Berggren, A. P. Chu, R. Younkin, and M. Prentiss, Science **280**, 1583 (1998).
[29] A. N. Boto, P. Kok, D. S. Abrams, S. L. Braunstein, C. P. Williams, and J. P. Dowling, Phys. Rev. Lett. **85**, 2733 (2000).
[30] G. P. Collins, Phys. Today **49**, 18 (1996).
[31] Y. Wu and R. Côté, Phys. Rev. A **65**, 053603 (2002).
[32] J. Evers, S. Qamar, and M. S. Zubairy, Phys. Rev. A **75**, 053809 (2007).
[33] K. T. Kapale, S. Qamar, and M. S. Zubairy, Phys. Rev. A **67**, 023805 (2003).
[34] V. Ivanov and Y. Rozhdestvensky, Phys. Rev. A **81**, 033809 (2010).
[35] R. G. Wan, J. Kou, L. Jiang, Y. Jiang, and J. Y. Gao, J. Opt. Soc. Am. B **28**, 10 (2011).
[36] R. G. Wan, J. Kou, L. Jiang, Y. Jiang, and J. Y. Gao, Opt. Commun. **284**, 985 (2011).
[37] R. G. Wan, J. Kou, L. Jiang, Y. Jiang, and J. Y. Gao, J. Opt. Soc. Am. B **28**, 622 (2011).
[38] L. L. Jin, H. Sun, Y. P. Niu, S. Q. Jin, and S. Q. Gong, J. Mod. Opt. **56**, 805 (2009).
[39] B. P. Hou, S. J. Wang, W. L. Yu, and W. L. Sun, J. Phys. B **38**, 1419 (2005).
[40] A. J. Li, X. L. Song, X. G. Wei, L. Wang, and J. Y. Gao, Phys. Rev. A **77**, 053806 (2008).
[41] P. Meystre and M. Sargent III, *Elements of Quantum Optics* (Springer-Verlag, Berlin, 1999).
[42] D. A. Steck, Rubidium 87 D line data, available online at [http://steck.us/alkalidata].
[43] H. R. Noh and H. S. Moon, Opt. Express **19**, 11128 (2011).
[44] Y. P. Zhang, A. W. Brown, and M. Xiao, Phys. Rev. Lett. **99**, 123603 (2007).
[45] J. T. Chang, J. Evers, M. O. Scully, and M. S. Zubairy, Phys. Rev. A **73**, 031803(R) (2006).
[46] M. O. Scully and M. S. Zubairy, *Quantum Optics* (Cambridge University Press, Cambridge, UK, 1997).
[47] L. L. Jin, H. Sun, Y. P. Niu, and S. Q. Gong, J. Phys. B **41**, 085508 (2008).